Forward-backward particle correlation measurements in proton-carbon collisions at 2.1 GeV

R. N. Treuhaft,* J. V. Geaga,† R. Koontz, H. G. Pugh, G. Roche,‡ and L. S. Schroeder
Nuclear Science Division, Lawrence Berkeley Laboratory, University of California, Berkeley, California 94720

C. L. Ruiz,§ J. Engelage, P. N. Kirk, and G. Krebs
Department of Physics and Astronomy, Louisiana State University, Baton Rouge, Louisiana 70803

J. W. Harris
Gesellschaft für Schwerionenforschung, D-6100 Darmstadt, Federal Republic of Germany
(Received 20 December 1983)

A (p,2p) experiment was carried out at 2.1 GeV to search for interactions between the incident proton and a fast dinucleon constituent inside the target nucleus. The results of this experiment along with a Two-Armed Spectrometer System used to make these coincidence measurements are described. Data are presented that indicate a possible contribution to the backscattered proton spectrum from such a dinucleon structure, although effects of statistics and experimental resolution allow only an upper limit to be set on the magnitude of this contribution. Effects of phase space, Fermi motion, and final state interactions on these measurements are discussed. A comparison with an intranuclear cascade model is shown. The systematics of other two-particle coincidence spectra obtained in this experiment are also presented.

I. INTRODUCTION

The results of an experiment[1] to study the correlation between particles (π^+,p,d) produced at forward laboratory angles of 10.4°, 45°, and 60° and target-related fragments (p,d) produced at 120° in 2.1 GeV proton-carbon collisions are reported. Similar experiments[2–4] have been conducted at energies below 1 GeV; but this is, to the best of our knowledge, the highest energy at which such electronic measurements have been undertaken. The forward- and backward-going particles were detected in coincidence in the Two-Arm Spectrometer System (TASS) at the Lawrence Berkeley Laboratory's Bevatron. Primary emphasis in the experiment was focused on the (p,2p) measurements to search for indications of the incident proton scattering from a two-nucleon cluster, "quasi or nuclear deuteron," in the carbon nucleus. Comparisons of the (p,2p) data with predictions of an intranuclear cascade and a phase space model are presented. In addition, a brief discussion of other two-particle correlations [(p,π^+p), (p,dp), and (p,pd)] is given.

The motivation for this experiment comes from two sources: early experiments studying production of high-energy protons emitted in the backward hemisphere in proton-nucleus and nucleus-nucleus collisions[5–9] and a lower energy (p,2p) experiment at 640 MeV by Komarov *et al.*[2] Since backward-going nucleons are kinematically forbidden in free nucleon-nucleon scattering, it was thought that the large momenta (typically 300—700 MeV/c) observed in single-particle inclusive experiments might arise from high-momentum components of nucleons in the target nucleus. Such high-momentum components can arise from a strong spatial dependence of the nucleon's wave function on other nucleons in the nucleus. This naturally gives rise to the idea of spatially correlated nucleon clusters. An incident nucleon scattering from such a correlated cluster could produce particles in kinematic regions inaccessible to free nucleon-nucleon collisions. These hypotheses were suggested to explain the yield of backward-going inclusive protons from proton-nucleus and nucleus-nucleus collisions.[9] Protons were observed with momenta far beyond the typical Fermi momenta measured in (e,p) experiments.[10] The (p,2p) study at 640 MeV by Komarov *et al.*[2] concluded that approximately one-third of the protons emitted backwards could be explained on the basis of a model involving the scattering of the incident proton from a dinuclear pair in the target nucleus.

An alternative to the hypothesis of scattering from correlated pairs as the source of the observed high-energy backward protons is quasi-two-body scaling (QTBS), first suggested by Frankel[11] and recently expanded by Gurvitz.[12] It was initially believed that QTBS describes the situation in which the incident proton scatters from a single fast, backward-going nucleon, the remaining A-1 nucleons recoiling coherently. When two particles are measured in the final state, QTBS produces results only slightly different from the correlated pair hypothesis. However, the high-momentum backward proton yield could also result from a series of multiple scatterings on two or more uncorrelated nucleons in the nucleus. Phase space calculations show that, for a (p,2p) experiment, the many-body final state expected to result from multiple scattering is very different from that resulting from either a correlated pair or the QTBS mechanism.[1]

The purpose of this experiment was to determine whether the mechanism of scattering from a correlated pair as indicated by Komarov *et al.*[2] was present at in-

cident energies above 1 GeV. The experiment was designed around the kinematic signal for scattering from a pair of nucleons in the nucleus, i.e., an enhancement in the coincidence cross section near free proton-deuteron (p-d) kinematics (throughout this paper the labels proton deuteron or proton pair refer to the same kinematics and are taken to be equivalent). As discussed in Sec. II for this experiment, the signal for scattering from a nuclear pair (observing free p-d kinematics for pd→ppn) is the observation of one or two peaks in the momentum spectrum of the forward-going particle. There were several reasons for choosing the incident energy to be 2.1 GeV. Firstly, the higher energy should provide a shorter wavelength probe of the short-range behavior of nucleons in nuclear matter. Secondly, there was an indication from measurements of backward pion production[13] that the production mechanism undergoes a change in going from incident energies below 1 GeV to energies above 1 GeV. If such a change is present, then a (p,2p) experiment at 2.1 GeV could be sensitive to it. Note that at the higher energy, the available phase space opens up substantially. In particular, at 2.1 GeV pion production processes account for over half the total nucleon-nucleon cross section, thereby providing additional mechanisms that could affect the backward inclusive-proton spectrum. Finally, there were two other two-particle correlation experiments[3,4] being done at 800 MeV that were studying the mechanism of proton production in the backward hemisphere.

The remaining plan of this paper is as follows:

(1) Section II outlines the kinematic regions associated with the free p-d reaction with and without Fermi motion, the kinematic region covered by this experiment, and the phase space associated with the other mechanisms mentioned above.

(2) Section III describes the spectrometer system (TASS) used to make these measurements, along with associated calibrations.

(3) Section IV reports the results of the experiment and interpretations relative to phase space considerations, the predictions of the intranuclear cascade code of Cugnon *et al.*,[14] and the effect of high-momentum components on the data. We also report our results for other two-particle coincidence channels studied.

(4) Section V summarizes our overall conclusions.

II. KINEMATICS FOR THE EXPERIMENT

A. Three-body kinematics (pd→ppn)

Although the target used in this experiment was carbon, the TASS magnets were set to detect the two protons in the final state of the reaction ^{2}H(p,2p)n. Assuming a stationary deuteron, values for five independent variables are required to specify the final state of this reaction. We chose the five independent variables to be the following: p_b, θ_b, ϕ_b, θ_f, and ϕ_f, where the subscripts "f" and "b" denote the forward and backward moving protons, respectively, p the laboratory momentum, and θ and ϕ the usual polar and azimuthal angles. The two azimuthal angles ϕ_f and ϕ_b were fixed at small ranges of values about 0° and 180°, respectively. For data-taking runs the polar angle of the backward-moving proton θ_b was fixed at 120°. The momentum of the forward-moving proton p_f can be calculated as a function of its polar angle θ_f and the momentum of the backward-moving proton p_b. The results of this calculation for an incident energy of 2.1 GeV are exhibited in Fig. 1 for $\theta_b=120°$ for fixed values of p_b represented by the contours. The contour represented by a single dot in Fig. 1 corresponds to the elastic scattering reaction p + d→p + d, for which $p_b=657$ MeV/c and $p_f=1.62$ GeV/c, half the momentum of the recoil deuteron at 10.4°.

If the reaction of interest, ^{2}H(p,2p)n, does, in fact, contribute to the cross sections measured in this experiment, then its effects should be observable as enhancements in the cross section at specific values of p_f. Consequently, the angular settings of the two magnets and the values for their central fields were chosen in such a way as to look for these enhancements at the prescribed values of p_f and for their absence at other values of p_f. The values so chosen are presented in Table I.

The simple considerations above are considerably complicated by inelastic processes such as pion production, as indicated in Fig. 2. The solid line in Fig. 2 corresponds to the contour for $p_b=400$ MeV/c taken from Fig. 1. The dotted line shows the contour that results from assuming that the observed reaction was not ^{2}H(p,2p)n but ^{2}H(p,2p)X, where X has a mass of 1078 MeV corresponding to an unobserved pion and nucleon going off together. The dashed line shows the contour for the reaction in

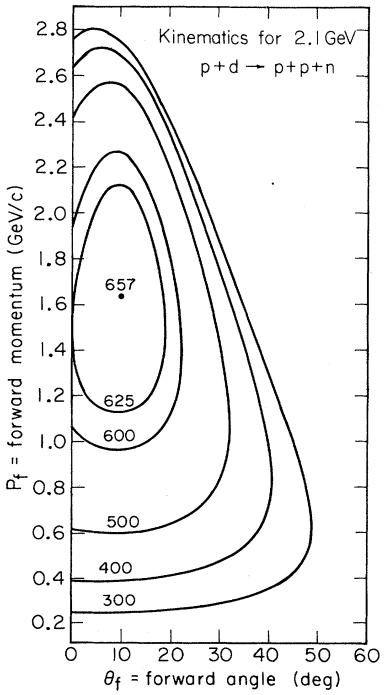

FIG. 1. Results of the solutions in terms of the forward proton momentum and angle for proton-pair kinematics from the reaction pd→ppn at 2.1 GeV. The backward proton being detected at $\theta_b=120°$. The contours are of constant backward momentum.

TABLE I. Magnet settings for data-taking runs.

Central angle front arm (deg)	Central angle rear arm (deg)	Range of momentum front arm (MeV/c)	Range of momentum rear arm (MeV/c)
10.4	120	400–900	400–850
10.4	120	800–1800	400–850
10.4	120	1500–3200	400–850
45.0	120	300–640	290–625
45.0	120	600–1400	290–625
60.0	120	300–640	290–625

which the unobserved system has the mass of the $\Delta(1232)$. Other such processes can be readily envisaged. All such inelastic processes would tend to broaden or shift the position of the expected enhancement.

B. Phase space and Fermi momentum

As previously observed, in the ^{2}H(p,2p)n reaction for every value of θ_f there are two values of p_f at which enhancements of the measured cross section might reasonably be expected on the basis of three-body kinematics. To determine which of these two values of p_f has the larger statistical weight a calculation of the available volume in phase space was carried out. This calculation was a generalization of the earlier work of Ruiz *et al.*,[15] in that the present calculation allowed for four- and five-body final states and incorporated the specific geometry of TASS. More importantly, Fermi momentum of the nuclear deuteron was included. The present computations were carried out in the laboratory frame of reference.

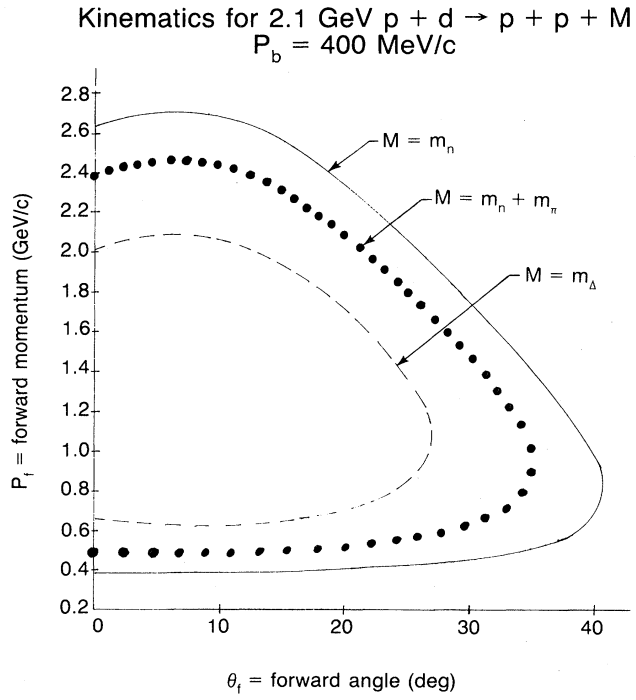

FIG. 2. Proton-pair kinematics at 2.1 GeV for different values of the unobserved mass M when the backward proton momentum is 400 MeV/c. The solid line corresponds to $M=m_N=938$ MeV, the dotted line to $M=m_N+m_\pi=1078$ MeV, and the dashed line to $M=m_\Delta=1232$ MeV.

If the struck deuteron is left in its ground state but allowed to have energy momentum characterized by a four-vector (E_d,p_d), then values for eight of the independent variables must be specified to solve for all the unknowns. The eight independent variables were chosen to be the following: p_b, θ_b, ϕ_b, p_f, θ_f, ϕ_f, θ_d, and ϕ_d, where θ_d and ϕ_d denote the polar and azimuthal angles of the deuteron. After a value for p_d was calculated by solving the equations for energy-momentum conservation, the initial state of the reaction was assigned a probability. Following Goldhaber,[16] we assumed that the probability for finding a fragment with momentum p_d and N_d nucleons inside a nucleus of atomic number A is proportional to $e^{-(p_d^2/2\sigma_d^2)}d^3p_d$, where

$$\sigma_d^2=\frac{N_d(A-N_d)\sigma_0^2}{A-1}$$

and

$$\sigma_0=90\ \text{MeV}/c\ .$$

The weighted volume in phase space for a nuclear deuteron with a momentum $p_d=(p_i-p_b-p_f-p_u)$ is then

$$R_3(\underline{p_i})=\int \frac{d^3p_b}{2E_b}\frac{d^3p_f}{2E_f}\frac{d^3p_u}{2E_u}e^{-(p_d^2/2\sigma_d^2)}d^3p_d \times\delta^4(\underline{p_i}+\underline{p_d}-\underline{p_b}-\underline{p_f}-\underline{p_u})\ ,$$

where the underlines denote four-vectors, and the subscripts "i" and "u" denote the incident and unobserved particles, respectively. A convenient form for the differential phase space for comparison with experimental cross sections is

$$\frac{d^4R_3(p_i)}{dp_b d\Omega_b dp_f d\Omega_f}=\frac{(p_bp_f)^2}{8E_bE_f}\int\frac{p_d^{*2}}{E_u^*}e^{-(p_d^{*2}/2\sigma_d^2)}d\Omega_d|D_3|\ ,$$

where D_3 is given by

$$D_3=\left[\frac{p_d^*}{E_d^*}-\frac{p_d^*}{E_u^*}-\frac{p_i\cos\theta_d}{E_u^*}+\frac{p_f\cos\theta_{d,f}}{E_u^*}+\frac{p_b\cos\theta_{d,b}}{E_u^*}\right]^{-1}$$

and

$$\cos\theta_{x,y} = \cos\theta_x \cos\theta_y + \sin\theta_x \sin\theta_y \cos(\phi_x - \phi_y) .$$

Asterisks are used as superscripts in the preceding equations to emphasize that the quantities to which they are attached are implicit functions of the independent variables. The integral in the preceding expression for the differential phase space was evaluated by Monte Carlo techniques for the reaction of interest, ^{2}H(p,2p)n, with $\theta_b = 120°$ and $\theta_f = 10.4°$. The results are shown in Figs. 3(a)—(c). Each of the three figures correspond to a different range of p_b, as indicated. The error bars on the points represent the statistics of the Monte Carlo calculation only. The arrow on each figure corresponds to QTBS kinematics and will be discussed later. The conclusion to be drawn from Fig. 3 is that the high momentum solution for p_f is favored by phase space.

To isolate the effects due to the Fermi momentum of the nuclear deuteron, a calculation with the width parameter $\sigma_d = 0$ was carried out, and the results are shown by the solid lines in Fig. 3(b). Without Fermi momentum there is a clear separation between the two solutions, but the solution with high momentum is still favored.

To determine how these results would be modified by background from reactions other than ^{2}H(p,2p)n, an expression for the differential N-body phase space was derived. The result is

$$\frac{d^4R_n(p_i)}{dp_b d\Omega_b dp_f d\Omega_f} = \frac{(p_b p_f)^2}{8E_b E_f} \int \frac{p_d^{*2} e^{-(p_d^{*2}/2\sigma_d^2)}}{E_1^*} d\Omega_d \times \prod_{j=2}^{N-2} \frac{d^3p_j}{2E_j} |D_N| ,$$

where

$$D_N = \left| \frac{p_d^*}{E_d^*} - \frac{p_d^*}{E_1^*} - \frac{p_i \cos\theta_d}{E_1^*} + \frac{p_f \cos\theta_{d,f}}{E_1^*} + \frac{p_b \cos\theta_{d,b}}{E_1^*} + \sum_{j=2}^{N-2} \frac{p_j \cos\theta_{d,j}}{E_1^*} \right|^{-1} .$$

The integral in the equation above was evaluated by Monte Carlo techniques for the specific geometry of TASS. In Figs. 4(a)—(c) we exhibit the available phase space for several reactions of interest. Single pion production through the reaction p + d→p + p + n + π is shown in Fig. 4(a), and the production of two pions is shown in Fig. 4(b). In both these calculations the nuclear deuteron was assumed to carry the Fermi momentum distribution specified in the discussion of Fig. 3, and the momentum of the backward-moving proton was required to satisfy the inequality 400 MeV/c < p_b < 500 MeV/c. In Fig. 4(c) we show the phase space for the reaction p + t→p + p + n + n. The Fermi momentum of the nuclear triton was taken to be a Gaussian with a standard deviation of 120 MeV/c. From Fig. 4 one sees that inelastic processes widen the momentum spectrum and shift the peak toward smaller values of momentum.

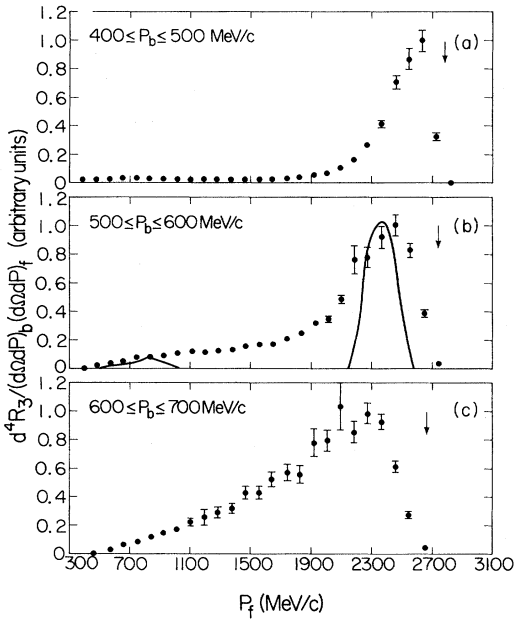

FIG. 3. Results of a Monte Carlo calculation (see the text) of the proton-pair differential phase space versus the momentum (p_f) of the forward going proton for pd→ppn at 2.1 GeV. In each case the internal momentum of the nuclear deuteron inside the target nucleus was assumed to be $\sigma_d = 120$ MeV/c. The different curves correspond to various cuts on the momentum of the backward proton: (a) 450—500 MeV/c, (b) 500—600 MeV/c, and (c) 600—700 MeV/c. The solid line in (b) indicates what happens when $\sigma_d = 0$ MeV/c. In all cases the error bars are statistical only. The arrow indicates the kinematic limit.

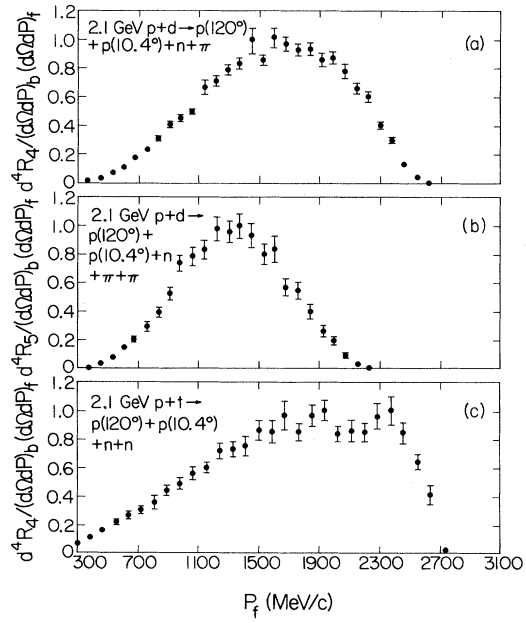

FIG. 4. Differential proton-pair phase space versus front momentum for various initial and final states: (a) pd→ppnπ, (b) pd→ppn$\pi\pi$, and (c) pt→ppnn. For each case: $\theta_b = 120°$, $\theta_f = 10.4°$, $400 \leq p_b \leq 500$ MeV/c, and $\sigma_d = 120$ MeV/c. Errors shown are statistical.

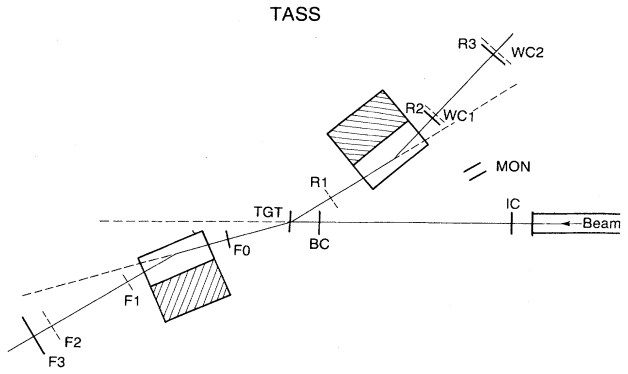

FIG. 5. Diagram of the Two-Arm Spectrometer System (TASS). The beam enters from the right. On the rear arm, $R1$ is a three-element scintillator hodoscope, $R2$ and $R3$ are scintillator gating counters, and $WC1$ and $WC2$ are multiwire proportional chambers. On the forward arm, $F0$ and $F3$ are scintillator gating counters, with $F1$ and $F2$ being 16-element scintillator hodoscopes. MON refers to a scintillator monitor telescope used for relative normalization. IC is the ion chamber used for absolute normalization of the experiment and BC the beam chamber used for measuring beam location and profile at the target.

III. APPARATUS AND EXPERIMENTAL PROCEDURE AND CALIBRATIONS

A. Hardware

A schematic of TASS is shown in Fig. 5, with the beam entering the apparatus from the right. The absolute intensity of the beam was measured by a calibrated ion chamber (labeled IC) on a spill-by-spill basis and stored along with other data on magnetic tape. Beam intensities varied from $\sim 5\times 10^8$ to 10^{10}/sec for coincidence measurements. The coordinates and profile of the beam at the target were measured by a beam chamber (BC). The beam chamber contained 32 horizontal wires and 32 vertical wires with a 2 mm spacing. These wires were individually read out for each spill and stored on magnetic tape as part of the data.

The apparatus contained two identical "C" magnets that rotated independently around a common pivot. The dimensions of the pole tips were 40.64 cm$\times$91.44 cm, and the gaps of both magnets were fixed at 20.32 cm. The distance from the center of the target to the pole tips was 1.07 m. The magnetic field in each magnet pointed downward and had a peak value of $\sim$20 kG.

The rear arm of TASS contained a scintillation counter hodoscope $R1$ with three elements. Two single scintillators, $R2$ and $R3$, were located behind the magnet. The rear arm also contained two multiwire proportional chambers (MWPC's), both of which had a 2 mm wire spacing. The front arm of TASS contained two scintillation counter hodoscopes, $F1$ and $F2$, each containing 16 elements. In addition, there were two single scintillators, denoted by $F0$ and $F3$. Table II summarizes the dimensions of each of these detectors and their distances from the center of the target as measured along the central trajectories.

B. Electronics

The fast triggering logic in this experiment is indicated schematically in Fig. 6. The three elements of $R1$ are labeled $R1A$, $R1B$, and $R1C$. Each of the single scintillators, $R2$, $R3$, and $F3$, was viewed by two photomultipliers, which are labeled A and B in each case. The symbol $F1$ in Fig. 6 represents a signal from at least one of the 16 elements of the hodoscope $F1$, and the symbol $F2$ is defined similarly with respect to the hodoscope $F2$. In this experiment an "event" was defined by the output from the majority logic unit. Consequently, events could be generated either by unaccompanied particles in either arm of TASS or by a coincidence between the two arms, depending on the setting of the switches on the module. The principal data-taking mode was the coincidence mode, which is denoted by $R\cdot F$ in Fig. 6. The acquisition of data was controlled by a PDP 11/34 computer through a multibranch driver (MBD).

An event as defined in this way was recorded only if the computer was not busy processing the preceding event. Approximately 600 μsec were required to process an event not including the time required to write the buffer on tape. A maximum of 310 events per second could be recorded, but most of the data taken in this experiment occurred at rates far below this maximum. A typical dead time for most runs was 10%, although struc-

TABLE II. Dimensions and positions of detectors.

Detector	Distance from center of target (cm)	Width (cm)	Height (cm)	Thickness (cm)
$R1$	61.0	3.8	7.0	0.24
$R2$	231.0	21.0	15.2	0.32
$WC1$	260.6	32.4	25.4	
$R3$	366.5	32.4	25.4	0.64
$WC2$	362.9	38.1	35.2	
$F0$	82.6	10.2	5.1	0.32
$F1$	239.2	20.3	10.2	0.32
$F2$	343.1	20.3	15.2	0.32
$F3$	369.7	20.3	15.2	0.64

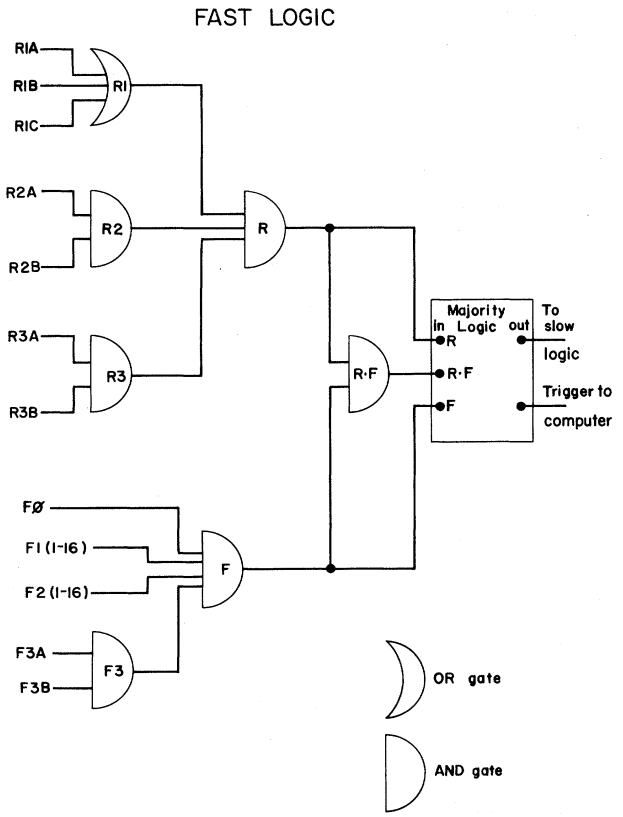

FIG. 6. Diagram of the fast logic used for this experiment.

ture in the beam spill increased the dead time significantly on occasion.

An assortment of analog and digital information was recorded for each event that occurred during the live time of the computer. The integrated output from the anode of every photomultiplier tube in the rear arm was recorded. Also recorded were the integrated outputs from the single photomultiplier tube attached to $F0$ and the two tubes attached to $F3$. Sixteen bit latches were associated with each of the hodoscopes $F1$ and $F2$. A third latch was associated with the other counters in the front arm, and a fourth with all the counters in the rear arm. The output from each of these latches was recorded. A time-to-digital converter (TDC) was associated with each of the photomultiplier tubes in the rear arm and also with the tubes $F0$, $F3A$, and $F3B$. All these modules were started by the arrival of a pulse from $R1$. Each module was stopped by the arrival of a pulse from the counter with which it was associated. The outputs of these ten TDC modules were recorded. In addition to data from the counters the MWPC's were interrogated after every event and the locations of the struck wires recorded. Selected scalers were also recorded after every event. At the end of the spill all scalers were recorded along with the output from the BC and IC and the values of the currents in the two magnets.

C. TASS magnetic fields

Because of the small dimensions of the counters, as shown in Table II, only a portion of the available aperture of each magnet was used in this experiment. Within this portion, the magnetic field could be approximated as a uniform field with a magnitude equal to the magnitude of the field at the center of the magnet. The effective length of the field was taken to be 103.99 cm, a value approximately equal to the sum of the true length of the pole tips and one-half the gap spacing, in accordance with the standard theory of fringing fields.[17] The uniform field approximation was checked by extensive measurements with the floating wire technique, and found to be accurate within $\pm 1.5\%$ over the entire range of momentum accepted by the magnets.

D. TASS acceptance

The validity of the uniform field approximation simplifies the calculation of the acceptance of the apparatus. By neglecting corrections due to energy loss and multiple scattering, one can readily calculate the solid angle presented by the apparatus to a charged particle of some chosen momentum. The result of such a calculation for the rear arm of TASS is shown in Fig. 7(a). The quantity δ_b on the abscissa is the fractional deviation of the chosen momentum p_b from the central momentum p_{cb} of the magnet. Figure 7(b) shows analogous results for the front arm of TASS. The effects of the beam spot size were included in both calculations.

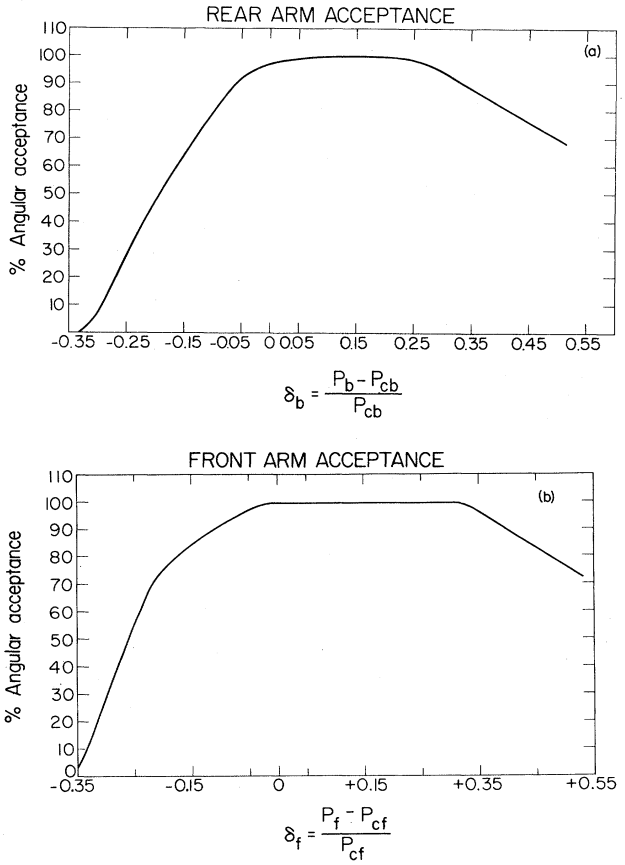

FIG. 7. Percent angular acceptance as a function of the deviation from central momentum setting for (a) rear and (b) front arms of TASS.

TABLE III. Characteristics of TASS.

	Rear arm	Front arm
Central momentum range	0–2150 MeV/c	0–2150 MeV/c
Momentum acceptance: $\Delta p/p_0$ (% of central momentum p_0)	−35–+50%	−35–+50%
Angular range (minimum angle between both arms = 70° in present configuration)	60°–180°	0°–60°
Angular acceptance: $\Delta\Omega$ (with counters listed in Table II)	4.3 msr	2.0 msr
Horizontal acceptance	2.77°	2.71°
Vertical acceptance	3.86°	2.43°
$\frac{\Delta p}{p_0}\times\Delta\Omega$	2.8 msr	1.7 msr
Momentum resolution	2.0%	4.4%
Angular resolution	0.25°	0.33°

To check the results of the numerical calculation and to evaluate the effects of energy loss and multiple Coulomb scattering, the acceptance for each arm of TASS was calculated independently by Monte Carlo techniques. Multiple Coulomb scattering was found to have a negligible effect on the values of the acceptance for the normal data-taking runs. Energy loss by ionization had a negligible effect for momenta greater than 600 MeV/c, and for momenta in the range between 300 and 600 MeV/c the magnitude of the correction did not exceed 3%.

Because of the small beam spot size the total acceptance of the spectrometer when operated in the coincidence mode was the product of the two single acceptances. Table III lists some of the overall characteristics of TASS.

E. Calibrations

Several calibrations of the apparatus were carried out. First, differential cross sections for proton-proton elastic scattering were measured for protons with kinetic energy of 1.05 GeV incident on a solid target of CH_2. Four measurements were made, three requiring coincidences between the two arms of TASS and one requiring only the detection of a single proton in the front arm of TASS. Values for any two independent variables, such as θ_f and ϕ_f, are sufficent to determine the final state of a two-body reaction, so the coincidence requirement overly constrained the kinematics. For this reason, the cross sections calculated from the coincidence data provided the most stringent test of our knowledge of the apparatus.

In Fig. 8 the elastic differential cross sections obtained from the coincidence data are shown as squares, and the cross section obtained from the front arm alone is shown as a triangle. For comparison the data of Dowell *et al.*[18] are represented by the solid circles. Our singles data are consistent with our coincidence data, but our values seem to be systematically lower than the data of Dowell *et al.*[18] This could partly be due to the 5% difference in beam energy. In our experiment the total systematic uncertainty in the cross sections derived from the coincidence data is estimated to be ±18%. The individual uncertainties that contributed to the total are an uncertainty of ±1% in the density of the target, an uncertainty of 3% in the magnitude of the correction due to nuclear absorption, an uncertainty of ±8% in the calibration of the ion chamber, an uncertainty of ±10% in the position of the detectors, and an uncertainty of ±13% in the angular settings of the two magnets. The magnitudes of the last two uncertainties are larger for these short calibration runs than they were for the normal data-taking runs because of the specific geometry in which these measurements were carried out.

In addition, inclusive cross sections were measured for the reaction $^{12}C(p,p)X$, with the single proton in the final state being detected in the rear arm of TASS set at an angle of 120° in the laboratory. Cross sections were measured for three currents in the rear magnet, with these currents chosen such that the resulting three ranges of momentum accepted by the magnet overlapped. Consequently, some of the same cross sections were measured for different values of the current in the magnet. Cross sections obtained from these measurements were com-

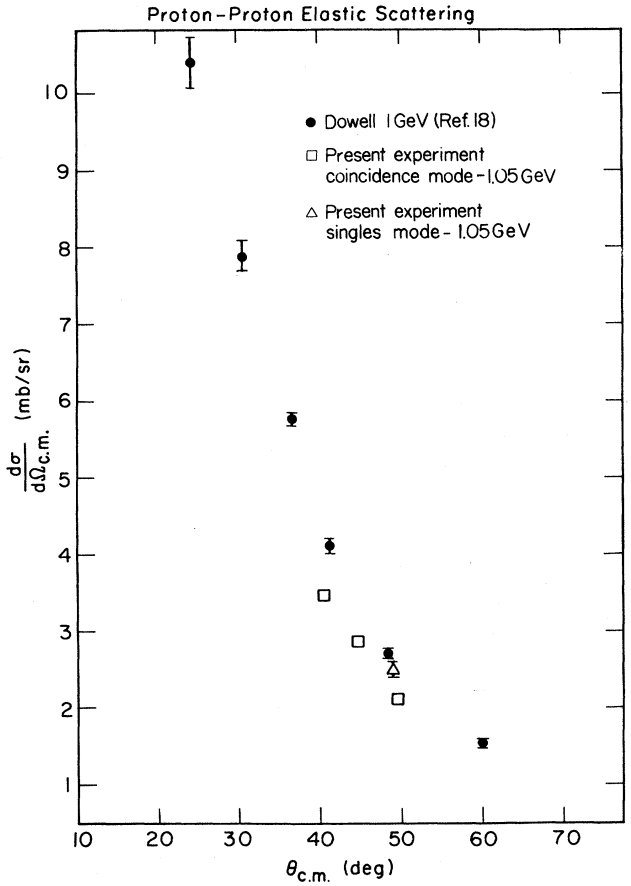

FIG. 8. Comparison of proton-proton elastic differential cross sections. Closed circles are data of Ref. 18 at 1 GeV, the squares (coincidence mode) and triangles (single-arm mode) are from the present experiment at 1.05 GeV.

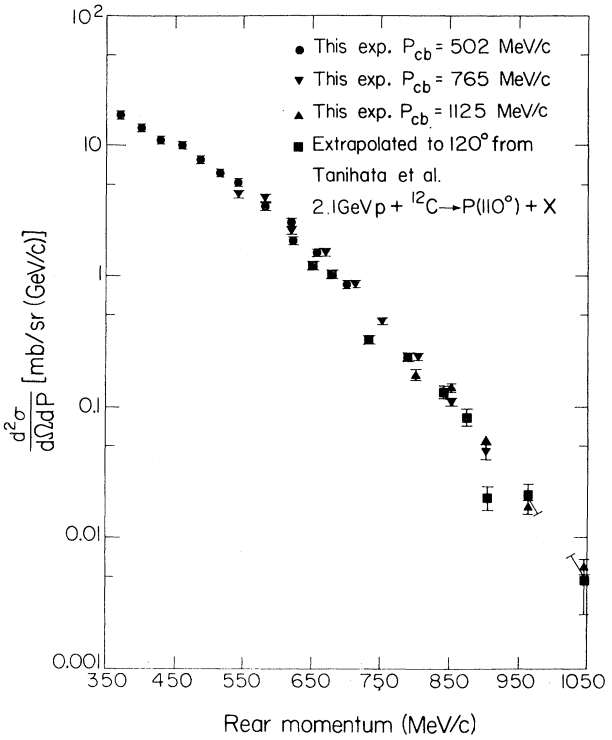

FIG. 9. Single-proton inclusive cross section at 2.1 GeV for $p + C \rightarrow p(120°) + X$ measured in the present experiment (circles and triangles) for different central value momentum settings. For comparison the data of Ref. 19 taken at the same energy but at 110° has been extrapolated to 120°.

pared with the single-particle inclusive data of Tanihata *et al.*[19] measured for the same reaction at 90° and 110° in the laboratory. We have extrapolated their data to 120° for the comparison shown in Fig. 9. Our data are seen to be in good agreement in both shape and magnitude with the extrapolated values of Tanihata.

F. Particle identification and background rejection

The time of flight (TOF) between selected counters was measured for each detected particle. These measurements were used in conjunction with the measurements of momentum to calculate the masses of the detected particles, and, in addition, they were the principal mechanism for the identification and rejection of random coincidences. In Fig. 10 we exhibit the mass separation that was achieved in the rear arm of TASS. The number on the abscissa is linearly proportional to the TOF between counters $R1$ and $R3$ in the rear arm. The scatter plot shows a distinct separation between protons and deuterons. Figure 11 shows the analogous scatter plot for the front arm of TASS. The number on the abscissa is linearly proportional to the TOF between the counters $F0$ and $F3$ in the front arm. The separation between protons and pions is more than adequate except perhaps for momenta greater than about 800 MeV/c. When the mass of the particle detected in the front arm is plotted against the mass of the particle detected in the rear arm, scatter plots such as the one in Fig. 12 result. The data separate nicely into distinct groups that correspond to the various combinations of masses.

In this experiment the principal problem was the extraction of the true coincidences from a substantial background of random coincidences. A typical beam spill was approximately 1 s in width and contained 10^9 protons. For such a spill the front arm of TASS detected 10^6 particles and the rear arm, 10^4 particles. Consequently, the principal type of background in this experiment consisted of coincidences between real but uncorrelated particles that originated from within the target but in different interactions.

TOF measurements are ideally suited to the rejection of such backgrounds. From the measurements of TOF in the rear arm it is a straightforward matter to calculate the time t_r at which the particle detected in the rear arm originated in the target. Similarly, the time t_f, defined with respect to the front arm, can be readily calculated. For particles that originated in the same interaction the quan-

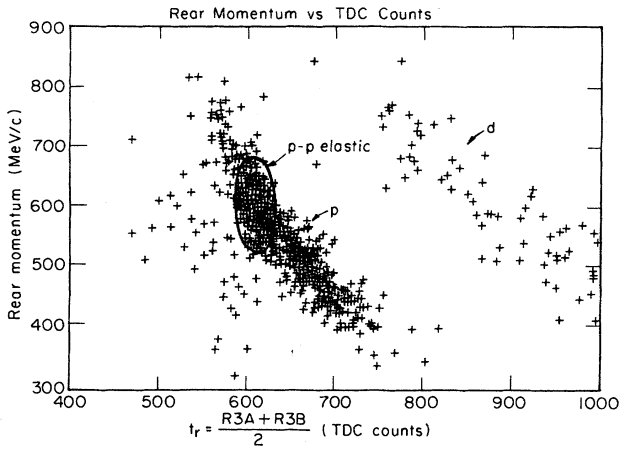

FIG. 10. Rear momentum versus raw TDC time-of-flight scatter plot.

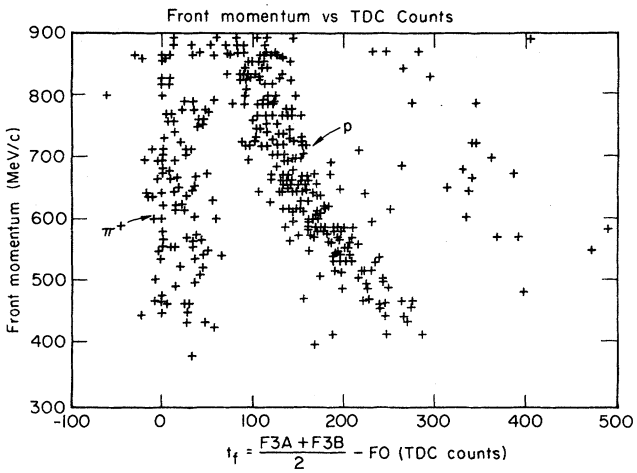

FIG. 11. Front momentum versus raw TDC time-of-flight scatter plot.

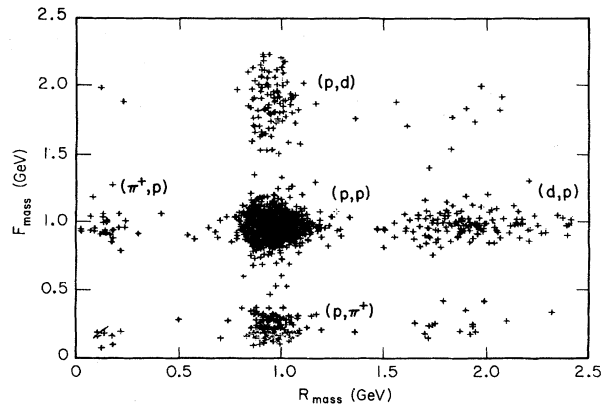

FIG. 12. Scatter plot of the particle masses determined when the two arms of TASS were operated in a coincidence mode. F_{mass} and R_{mass} are the masses of the particles in the forward and rear arms, respectively.

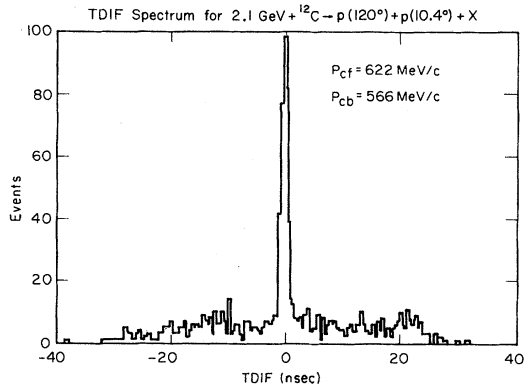

FIG. 13. Histogram of TDIF (see the text) for a (p,2p) run in this experiment with the forward arm set for a central momentum of 622 MeV/c and the rear arm at 566 MeV/c.

tity TDIF$=t_r-t_f$ will be approximately zero, but for random coincidences the values of TDIF will be distributed uniformly across the total time resolution of the electronics. Figure 13 shows such a histogram taken in a normal data run. The large peak with width 2 ns corresponds to true coincidences. For other data-taking runs in this experiment the ratio of true peak to random background varied between the values 6 and 10:1.

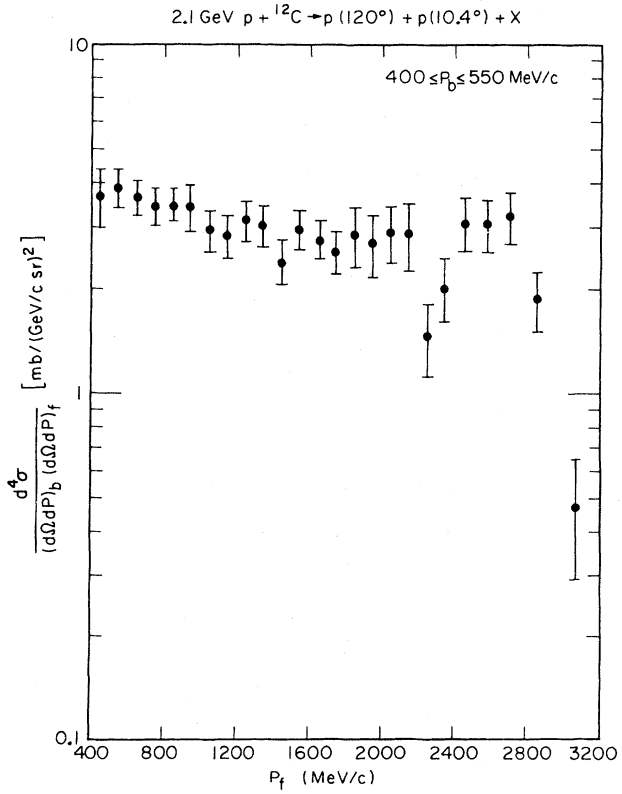

FIG. 14. Coincidence spectrum obtained for

2.1 GeV p+C→p(120°)+p(10.4°)+X

as a function of forward proton momentum. The rear proton momentum being in the interval $400 \le p_b \le 550$ MeV/c.

IV. EXPERIMENTAL RESULTS

We now turn to a discussion of the results of the coincidence measurements using 2.1 GeV protons on a natural carbon target.

A. C(p,2p)X measurements and systematics at 2.1 GeV (10.4° results)

We first display the differential cross section,

$$d^4\sigma/(d\Omega\, dp)_f(d\Omega\, dp)_b \ ,$$

versus front momentum (p_f) at $\theta_f = 10.4°$, for two different cuts on rear momentum. The backward angle is, as always, $\theta_b = 120°$. In each case, the contamination to the (p,2p) signal resulting from misidentification of the forward-going particle is estimated to be $< 5\%$. As indicated earlier, if the process pd→ppn contributes to the (p,2p) reaction being measured at 2.1 GeV, from Fig. 1 we expect to observe enhancements in the coincidence spectrum, one at a lower value of p_f and one at a higher value of p_f.

Figure 14 shows the coincidence spectrum for the rear momentum (p_b) cut, $400 \leq p_b \leq 500$ MeV/c. This spectrum is subject to a $\pm 17\%$ systematic uncertainty. The forward momentum spectrum is seen to be slowly falling from an average value of about 3.5 mb/(GeV/c sr)^2 at 800 MeV/c to an average value of 2.8 mb/(GeV/c sr)^2 at 1800 MeV/c. There is a dip at 2200 MeV/c followed by an increase to about 3 mb/(GeV/c sr)^2 at 2600 MeV/c and then an abrupt falloff above 2800 MeV/c. The sharp cutoff in this spectrum can be associated with the approach to various kinematic limits. For example, the kinematic limit in forward momentum for a coherent reaction like $p + {}^{12}C \rightarrow pp + {}^{11}B$ is 2779 MeV/c for an average backward momentum, $p_b = 475$ MeV/c. For this cut in backward momentum (referring to Fig. 1) we would expect to see enhancements for the process pd→ppn around $p \approx 600$ and 2600 MeV/c. Only the one corresponding to the high-momentum solution seems to be present. At our bombarding energy of 2.1 GeV, the probability of producing an undetected pion is large, and such a mechanism could well be dominating our measured spectrum [see Figs. 4(a) and (b), for example] at lower and intermediate values of p_f, thus totally obscuring the three-body process we seek to isolate.

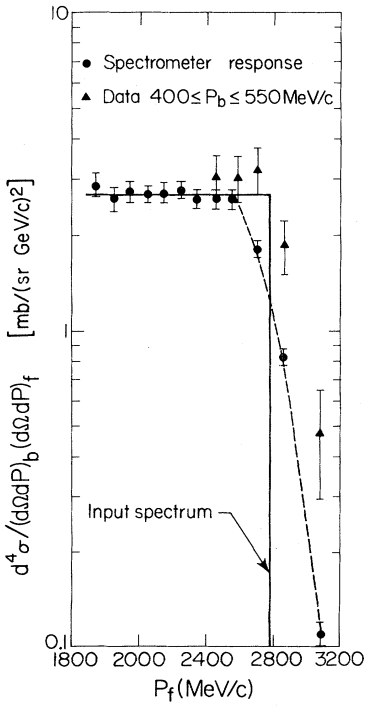

FIG. 15. Response of the forward arm of TASS to a flat input spectrum (solid line) out to the p-carbon kinematic limit of 2771 MeV/c (for $p_b = 475$ MeV/c). Circles represent the response of the spectrometer, with the dashed line serving as a guide to the eye for the input spectrum.

One could argue, ignoring the dip at 2300 MeV/c, that the spectrum of Fig. 14 is consistent with being flat until abruptly cutting off at the kinematic limit. Following this line of reasoning, Fig. 15 shows the response of TASS to a flat spectrum that cuts off at the forward momentum corresponding to the proton-carbon kinematic limit for a backward momentum of 475 MeV/c. The input spectrum (which cuts off just below 2800 MeV/c) is also shown. The flat part was normalized to an average value of the data of Fig. 14 between 1600 and 2800 MeV/c. Also shown are the last few data points from Fig. 14 for reference. The dashed line guides the eye through the Monte Carlo reconstructed points.

The data fall off at about 2800 MeV/c, 200 MeV/c higher than the reconstructed spectrum. Assuming no systematic front momentum error, the persistence of the high-momentum part of Fig. 14 implies that there must be an enhancement in the spectrum above a flat distribution, near the kinematic limit. The proton-proton elastic scattering calibration data indicate that the front momentum is accurate to $\pm 2\%$, insufficient to account for the observed effect. This analysis is supported by the presence of the marginally significant dip at 2300 MeV/c. The two effects, taken together, suggest a sizable peak at high forward momentum that has been obscured by low statistics and the moderate resolution of the forward arm.

An additional piece of information that bears on the question of the ability of the forward arm of TASS to resolve a peak at high momentum is displayed in Fig. 16. This figure shows the 2.1 GeV single-particle inclusive proton data of Ref. 19 taken at 10° together with data from the present experiment at 10.4°. During this particular data run we measured only the shape of the singles spectrum and have therefore normalized our data to that of Ref. 19 (2.1 GeV, $\theta_{lab} = 10°$) at $p_f = 1600$ MeV/c. The 10.4° singles taken with TASS clearly show an enhancement at the quasi-elastic peak, expected at $p_f = 2760$ MeV/c for 2.1 GeV proton-proton kinematics.

Next we display in Fig. 17 the forward momentum spectrum for a higher backward momentum cut of $550 \leq p_b \leq 700$ MeV/c. The systematic error in cross section here is $\pm 9.5\%$. The spectrum is essentially flat or slightly falling at low momentum. At high momentum it falls abruptly above 2500 MeV/c. Again, one can test to see if the spectrum at the high-momentum end is essen-

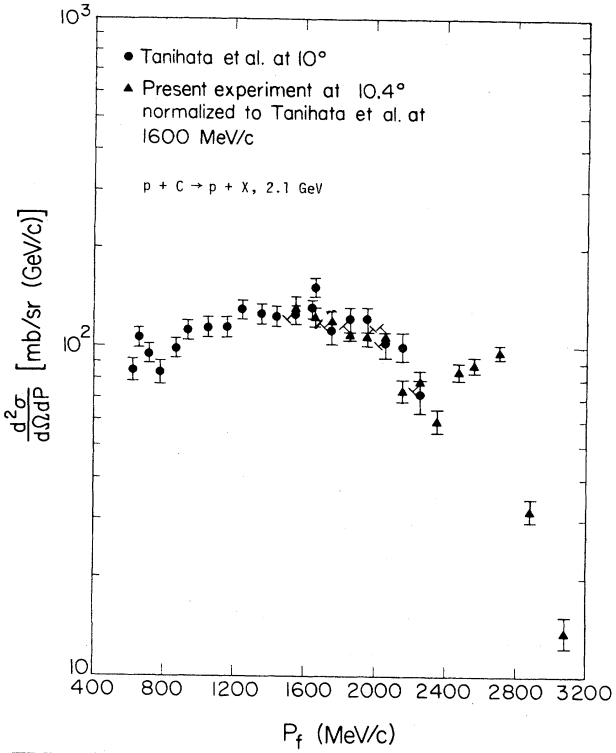

FIG. 16. Inclusive proton spectrum for 2.1 GeV proton-carbon interactions measured by the front arm of TASS. The present experiment (triangles) has been normalized to results of Ref. 19 (circles) for the purpose of comparison.

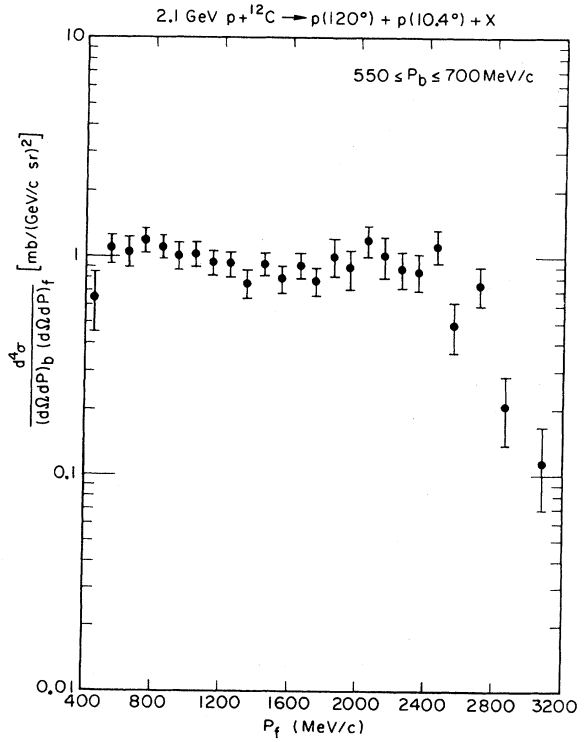

FIG. 17. Coincidence spectrum for

$$2.1\ \text{GeV}\ p+C\rightarrow p(120^\circ)+p(10.4^\circ)+X$$

as a function of the forward proton momentum. The rear proton momentum being in the interval $550 \leq p_b \leq 700$ MeV/c.

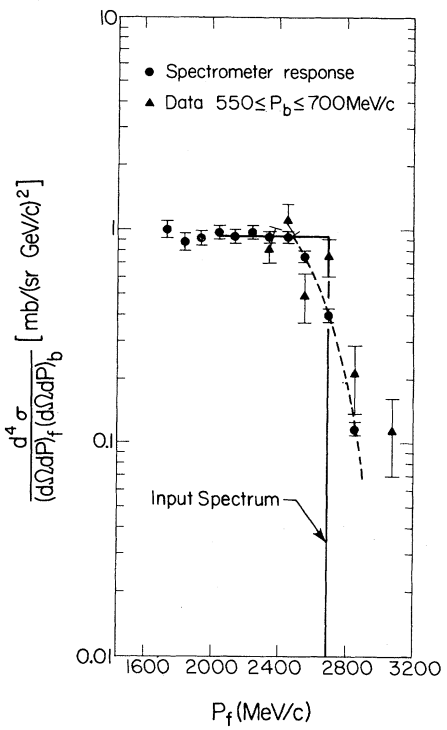

FIG. 18. Response of the forward arm of TASS to a flat input spectrum (solid line) out to the p-carbon kinematic limit of 2691 MeV/c (for $p_b = 625$ MeV/c). Circles represent the response of the spectrometer, with the dashed line serving as a guide to the eye for the input spectrum.

tially flat until it falls off at the kinematic limit of 2691 MeV/c, which corresponds to a backward momentum of 625 MeV/c. Figure 18 is the analog of Fig. 15 for the high rear momentum cut. Here the falloff point of the data and the reconstructed events are almost identical, indicating no hint of an enhancement from a three-body final state at high momentum.

Assuming there is a peak at the high forward momentum end of Fig. 14, what is its origin? By examining Figs. 3(a), 3(b), and 4 we are led to the conclusion that only an interaction of the incident proton with one or two nucleons, in the absence of pion production, can produce a kinematic peak in the high forward momentum region, above 2500 MeV/c. As previously stated, given the resolution of the front arm of TASS, it is difficult to tell if the possible "peak" of Fig. 14 results from a proton pair or proton-nucleon interaction. If one assumes, however, that the actual front momenta populated in the peak of Fig. 14 are due to a proton-nucleon interaction, then the real kinematic peak is only on the order of 100 MeV/c wide. If this were the case, the data of Fig. 14 are consistent with a peak of height 17 mb/(GeV/c sr)^2. This is to be compared to a value of 21.6 mb/(GeV/c sr)^2 quoted by Frankel *et al.*[3] in their study at 800 MeV.

However, if one allows for a final state interaction or coherent interactions with large parts of the nucleus, one can observe apparent few-body kinematics, even though a large number of nucleons participate. Frankel *et al.*[3] at-

tribute their quasi-elastic peak to such a coherent reaction in an experiment done at 800 MeV. In fact, any such kinematic search must be supplemented by dynamic considerations to resolve the multistep or final state interaction problem.

B. C(p,2p)X measurements at 45° and 60°

The coincidence cross section measured at $\theta_f = 45°$ and 60° cover front momenta very far from the kinematic limit (see Fig. 1). Figure 19 shows the coincidence cross section for the reaction

$$2.1 \text{ GeV } p + C \rightarrow p(120°) + p(45°) + X$$

for the two backward momentum cuts shown. The label "low field" means that the data were taken at a forward central momentum of 422 MeV/c, while the "high field" data were taken at a central momentum of 922 MeV/c. The low backward momentum cut spectrum is subject to 15% systematic error, and the high backward cut spectrum is subject to 9% systematic error.

The two backward momentum cuts of Fig. 19 show no statistically significant difference in shape, both slightly rising up to 500 MeV/c and falling off at higher momentum. Superimposed on Fig. 19 (with arbitrary normalization) is the shape of the singles spectrum ($d^2\sigma/d\Omega\, dp$) at a laboratory angle of 45° from Ref. 19. Both backward momentum cuts for coincidence spectra exhibit the same qualitative shapes as the singles data, which suggests that because of multiparticle cascades or final state interactions or both, there is little correlation between the forward- and backward-going protons for these momentum-angle combinations. Also note that the spectra do not show any enhancement near the p-d kinematics of Fig. 1. The effects of Fermi momentum and phase space have also been investigated, but they do not change the conclusion that the spectra show no direct evidence for a proton-pair contribution.

Figure 20 shows the coincidence cross sections at low forward momenta at $\theta_f = 60°$, which is beyond the kinematic region accessible to free proton-pair scattering as indicated by Fig. 1. The low forward momentum data at $\theta_f = 60°$ show the same trend as that of $\theta_f = 45°$ and are quite comparable in magnitude at their respective peaks. At higher momenta, the 60° data fall off more rapidly due to lack of available phase space. Because the 60° data are outside the free proton-pair kinematics, a substantial pair center-of-mass Fermi momentum is necessary to populate

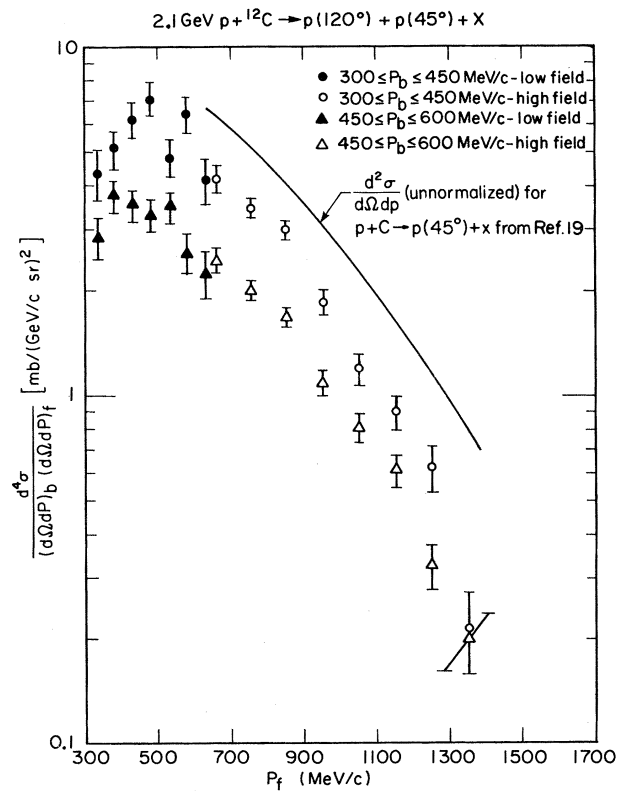

FIG. 19. Coincidence spectrum for

$$p + C \rightarrow p(120°) + p(45°) + X$$

at 2.1 GeV versus forward momentum for the listed cuts on back momentum. Low field and high field refer to different magnetic field settings of the forward arm. For comparison, the *shape* of the 45° single-proton inclusive spectrum (solid line) from Ref. 19 is also indicated.

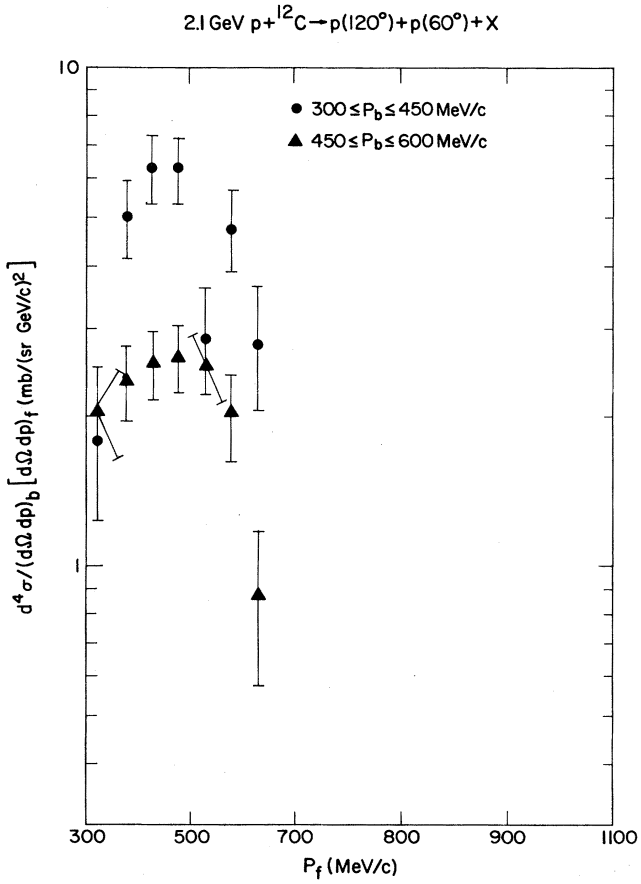

FIG. 20. Coincidence spectrum for

$$p + C \rightarrow p(120°) + p(60°) + X$$

at 2.1 GeV versus forward proton momentum for two different cuts on backward proton momentum.

the kinematic region of the 60° data. Pure phase space predicts that the pair interaction cross section should be down by a factor of 6 from the 45° data because of the low probability of finding the required pair Fermi momenta. The similarity in shape and magnitude of the 60° data to that of the low forward momentum 45° data again indicates that there is no direct evidence for a proton-pair contribution to the higher forward angle coincidence data.

C. Comparison of (p,2p) results with intranuclear cascade model

We now compare the (p,2p) data with the predictions of an intranuclear cascade model.[14] This model has input data in good agreement with nucleon-nucleon and pion-nucleon cross sections and is known to work well for nucleon collisions up to 2 GeV. Approximately 600 000 proton-carbon cascade events at 2.1 GeV were generated. The calculation was performed for impact parameters $b \leq b_{\max} = 3.76$ fm.

Figure 21 shows a comparison between our singles measurements and the cascade predictions. The backward singles spectrum in Fig. 21(a) is seen to be in remarkable agreement in both magnitude and shape with the cascade results. However, the forward singles spectrum in Fig. 21(b) disagrees in both magnitude and shape, particularly in the region of $p_f \sim 2400$–2800 MeV/c, where the quasi-elastic peak is expected. It is worth noting that a detailed examination of the cascade events indicates that $\sim 60\%$ of the protons appearing in the forward arm (taken to be $10.4° \pm 0.5°$ for purposes of the calculation) were found to be the scattered beam proton, having suffered ~ 2.2 collisions on the average. In the case of the backward-going protons ($120° \pm 10°$) only $\sim 6\%$ are identified as the original beam proton, having been involved in an average of ~ 3.7 collisions.

Figure 22 shows a comparison between the coincidence spectrum and the predictions of the intranuclear cascade calculation. Because of the coincidence requirement imposed on the cascade calculation, the number of cascade-generated events was greatly reduced compared to the number available for the singles comparison. The low-momentum cut contains 837 cascade events, while the high-momentum cut has 227 events. The uncertainties shown on the cascade predictions reflect the statistical errors. For values of $p_f < 1600$ MeV/c, the data and cascade are in approximate agreement in overall magnitude and shape, both data and model being relatively flat in this region. However, the intranuclear cascade greatly overpredicts the yield at high momenta by over an order of magnitude at the peak values. Detailed examination of the coincidence cascade events indicates that, as in the case of the singles events, $\sim 60\%$ of the forward-going and $\sim 6\%$ of the backward-going protons correspond to the beam proton. Since the cascade model has no built-in dynamical correlations between target nucleons, one

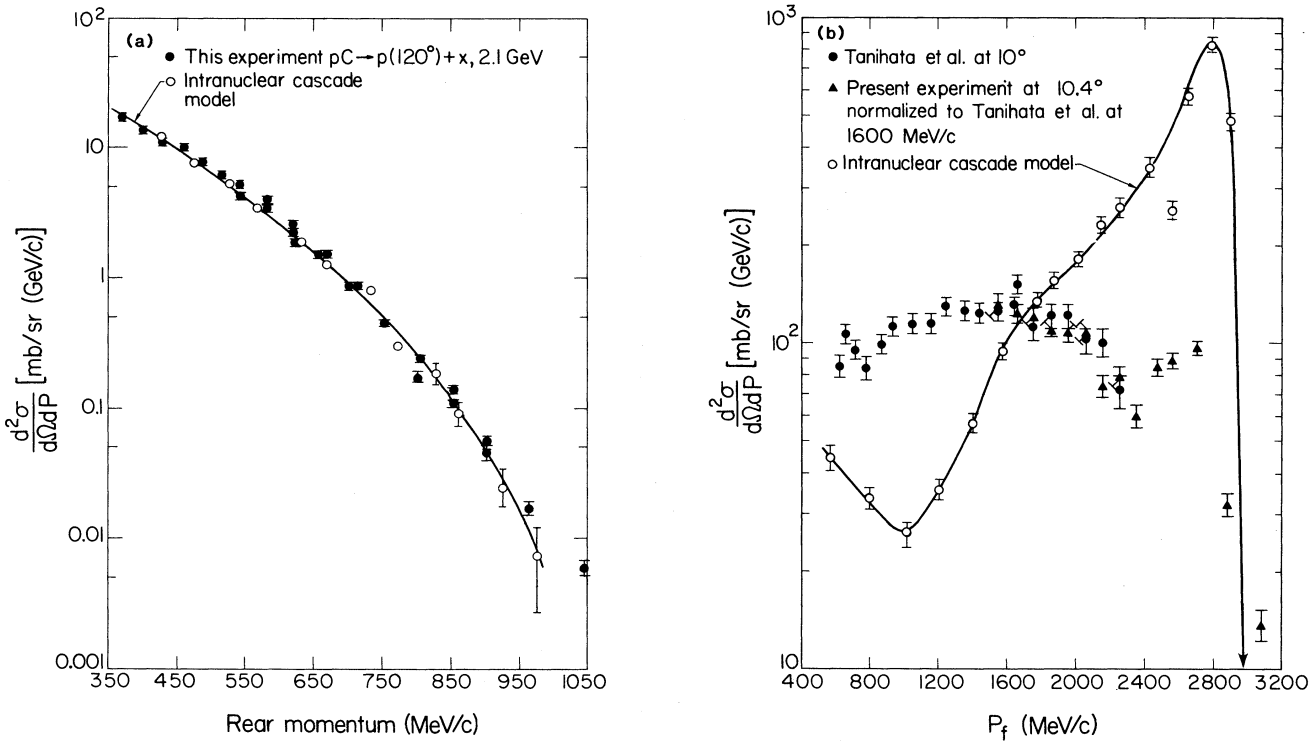

FIG. 21. Single-proton inclusive spectrum compared with results of an intranuclear cascade (INC) model as described in the text: (a) rear singles, $\theta = 120°$, and (b) forward singles, $\theta = 10.4°$. The errors associated with the INC model are statistical only. The solid line is a guide to the eye.

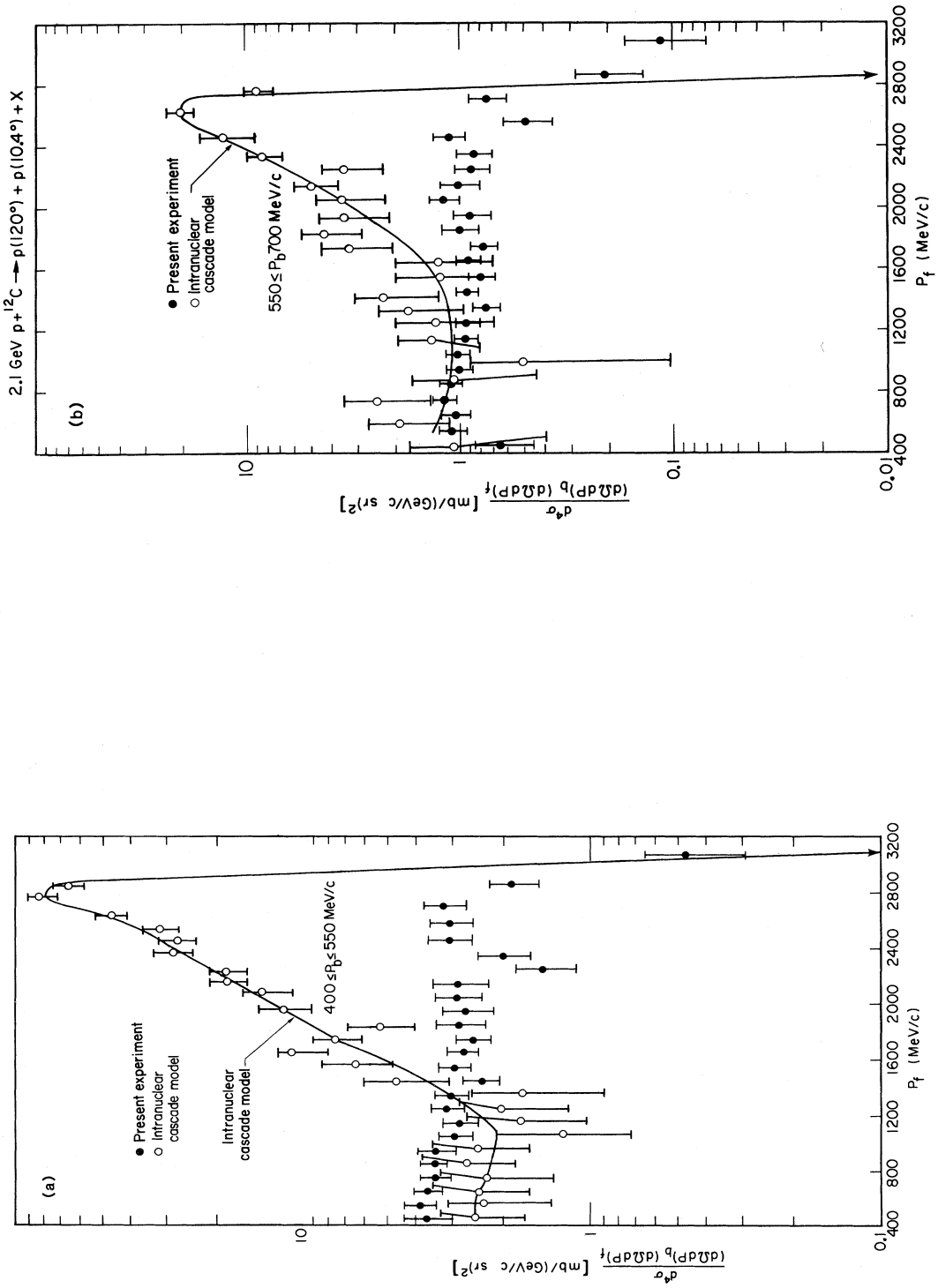

FIG. 22. Results of the intranuclear cascade (INC) model compared with the coincidence spectra from p+C→p(120°)+p(10.4°)+X at 2.1 GeV, for different cuts on backward proton momentum: (a) $400 \leq p_b \leq 530$ MeV/c, and (b) $550 \leq p_b \leq 700$ MeV/c. The solid line is a guide to the eye.

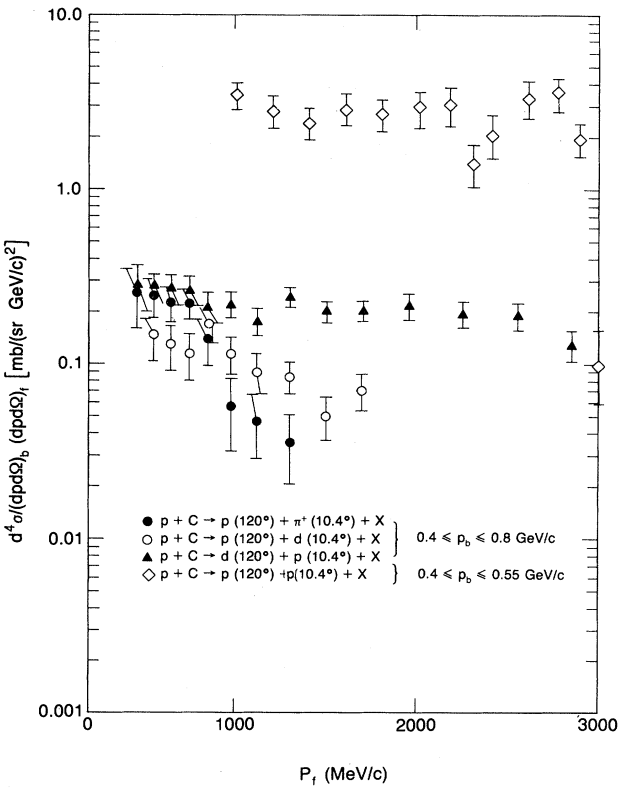

FIG. 23. Coincidence spectrum for various final state particles in proton-carbon collisions at 2.1 GeV for the indicated cuts on backward momentum. In each case, $\theta_f = 10.4°$ and $\theta_b = 120°$. Errors shown are statistical only.

would expect these percentages to be independent of whether one examines the singles or coincidence events. Finally, we note that in $\sim$30—40% of the events, both the forward and backward protons come from the target.

D. Other two-particle correlation measurements at 10.4°

Simultaneous with the (p,2p) experiment at 2.1 GeV, data were also collected for other two-particle coincidences. These other channels amounted to about 30% of the total two-particle trigger rate. Since the majority of the data were taken at $\theta_f = 10.4°$, only this set has been analyzed for reactions other than (p,2p). The other two-particle channels that have been observed with adequate statistics to report on are the following: (p,π^+p) with the positive pion in the forward arm; (p,dp) with the deuteron forward; and (p,pd) with the proton forward and deuteron in the rear arm. Again in all cases, $\theta_b = 120°$. Bear in mind that the experimental program was set up to scan in the region of p-d kinematics for the (p,2p) reaction, dictating our choice of angles and momenta. These choices have no particular dynamical significance for the three two-particle coincidence measurements mentioned above. However, their yields and shapes are of interest in themselves and can bear on the question of the mechanisms helping to populate the backward singles spectrum.

The lower portion of Fig. 23 shows the cross sections for these other channels versus the forward-going particle's momentum. For all cases, $\theta_f = 10.4°$, $\theta_b = 120°$, and each is displayed for a backward momentum cut of $0.4 \leq p_b \leq 0.8$ GeV/c. The (p,π^+p) and (p,dp) spectra are remarkably similar in magnitude and shape up to $p_f \approx 1000$ MeV/c. The (p,pd) spectrum, although comparable in magnitude, is much flatter and extends to high forward momenta like the (p,2p) spectrum. For the (p,pd) spectrum it is possible that the low-momentum end (below $\sim$1000 MeV/c) arises from protons that are target related. The high-momentum end could be associated with the incident proton scattering from a deuteron cluster that then proceeds backwards, i.e., a QTBS type of process. In this type of process, the proton would be expected to continue forward but at a momentum >2.89 GeV/c (which is the beam momentum). Formation and decay of an intermediate $\Delta(1232)$ state could, however, provide forward protons at reduced momenta.

The (p,2p) data are displayed in the upper portion of Fig. 23 for comparison with the other channels. The (p,2p) spectral shape shown is for the low-momentum cut indicated. It shows a falloff similar to the (p,pd) at higher momentum but with a much larger yield than the other two-particle spectra. This is, of course, to be expected since the experiment was optimized to look at the (p,2p) reaction.

Figures 24(a)—(c) shows the backward spectrum selected on different values of the momentum of the forward-going particle for the three reactions discussed. Other than the fact that the yields decrease with increasing p_f cuts, the spectra all exhibit remarkably similar shapes. This suggests that the forward and backward particle's spectra are essentially independent of each other. Statistical emission could account for such a process. However, with a system as light as carbon, one might expect to see some correlation. Again, a more thorough study in momentum and angle, as well as more complete information about the various final states, is required to pin down the contributing processes.

V. SUMMARY

The C(p,2p)X reaction has been studied at 2.1 GeV in a magnetic Two-Arm Spectrometer (TASS) at the Bevatron. Coincidences between forward (10.4°, 45°, and 60°) and backward (120°) protons were recorded and analyzed to look for evidence of the incident proton scattering from a two-nucleon substructure in the target. The salient features of the 10.4° data are the following:

(1) The low backward momentum spectrum suggests the presence of a peak near the kinematic limit. Statistics and the finite resolution of TASS do not allow us to determine whether this possible structure arises from proton-nucleon or proton-dinucleon scattering. An upper limit of 17 mb/(GeV/c sr)^2 on the peak height of this effect is set slightly lower than the value of 21.6 mb/(GeV/c sr)^2 observed at 800 MeV in a similar experiment.[3]

(2) The high backward momentum cut yields a result consistent with reaching the proton-carbon kinematic limit.

(3) Most of the coincidence spectra are insensitive to the

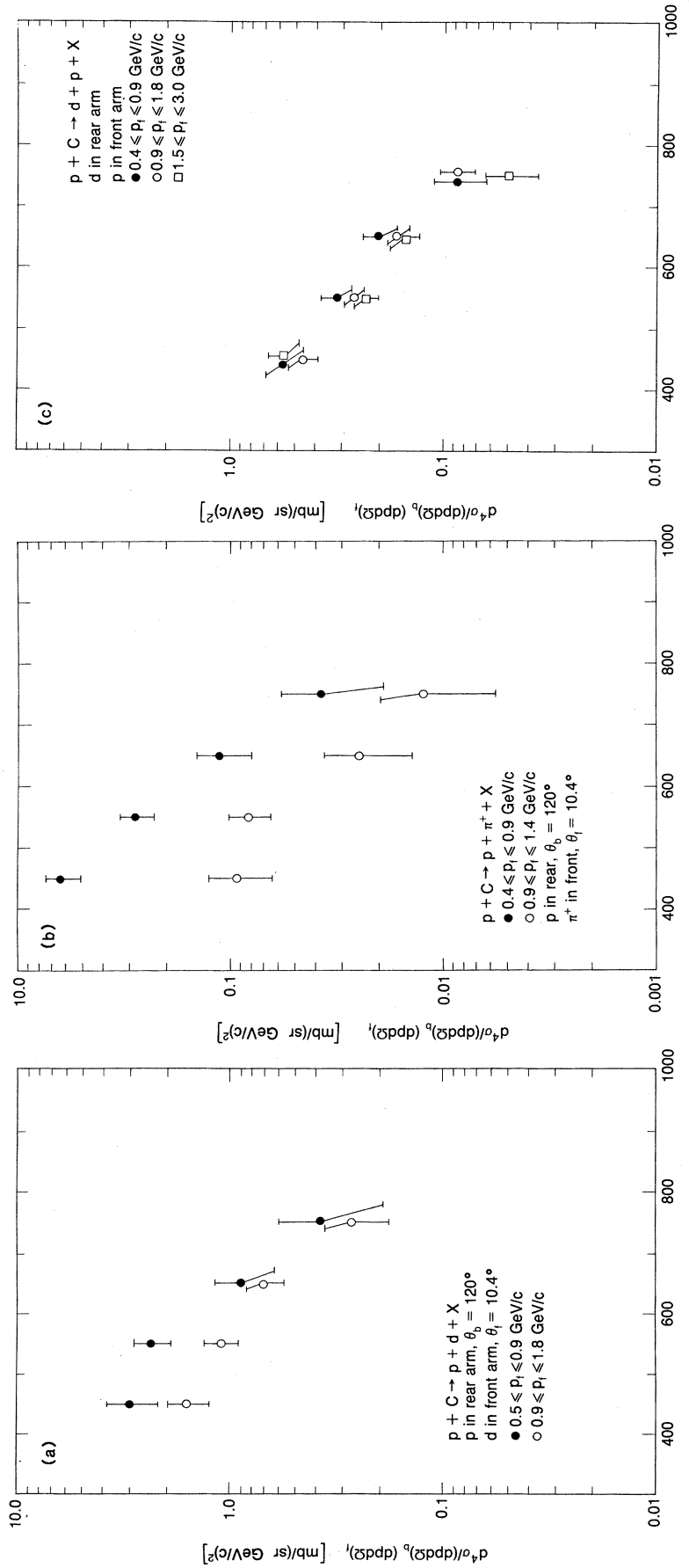

FIG. 24. Coincidence spectra for the different final states indicated: (a) $p + C \rightarrow p\pi^+ + X$, (b) $p + C \rightarrow pd + X$, (c) $p + C \rightarrow dp + X$ at 2.1 GeV as a function of the backward-going particle's momentum for various forward momentum cuts.

momentum cut in the backward or forward arms, suggesting that final state interactions or mechanisms with overlapping kinematic regimes make conclusions difficult away from the kinematic limit for the process pd→ppn.

(4) The spectrum below 2400 MeV/c is relatively structureless. This suggests that a variety of processes including highly inelastic collisions, scattering from nucleon clusters larger than two, along with multiple scattering and/or final state interactions, are responsible for this smooth spectrum. This is further borne out by comparison of the coincidence spectrum with the predictions of an intranuclear cascade model. A kinematically more complete experiment is required to ascertain the strength of these various contributions to the C(p,2p)X reaction.

The other two-body coincidence channels studied were found to be comparable in strength and shape, strongly suggesting that their emission patterns were dominated by statistical processes. Only the reaction

$$p+C\rightarrow p(\text{foward})+d(\text{backward})+X$$

shows signs of structure, possibly indicative of the forward proton arising as a result of target fragmentation at low proton momenta and as a quasi-elastic proton at high momenta.

By going to much higher energies than previous (p,2p) experiments, new reaction channels open up. Particularly important are those involving pion production. At 2.1 GeV it appears that a large number of competing processes are required to explain the backward singles proton rates observed in earlier experiments.

ACKNOWLEDGMENTS

We would like to thank the Bevatron crew, particularly Fred Lothrop, Bob Miller, and Jose Alonso, for providing the beam on target. We thank Everett Harvey for expert help in getting our computer system up and running. Particular thanks go to Al Smith, for his invaluable assistance in the ^{11}C activation studies used to calibrate our ion chamber. One of us (G.R.) was supported in part by IN2P3 and NATO grants. This work was supported by the U.S. Department of Energy under Contract DE-AC03-76SF00098 and by DE-AS05-76ER04699.

*Present address: Jet Propulsion Laboratory, Pasadena, CA 91109.

†Present address: Hughs Helicopter Inc., Culver City, CA 90230.

‡Present address: University of Clermont-Ferrand II, 63170 Aubiere, France.

§Present address: Sandia Corporation, Albuquerque, NM 87185.

[1]R. N. Treuhaft, Ph.D. thesis, University of California, Lawrence Berkeley Laboratory Report LBL-14677, 1982 (unpublished).

[2]V. I. Komarov, G. E. Kosarev, H. Muller, D. Netzband, V. D. Toneev, T. Stiehler, S. Tesch, K. K. Gudima, and S. G. Mashnik, Nucl. Phys. **A326**, 297 (1979).

[3]S. Frankel, W. Frati, C. F. Perdrisat, and O. B. Van Dyck, Phys. Rev. C **24**, 2684 (1981).

[4]Y. Miake, Ph.D. thesis, Institute for Nuclear Study Report INS-NUMA-39, 1982 (unpublished).

[5]J. R. Wu, C. C. Chang, and H. D. Holmgren, Phys. Rev. C **19**, 698 (1979).

[6]S. Frankel, W. Frati, O. Van Dyck, R. Werbeck, and V. Highland, Phys. Rev. Lett. **36**, 642 (1976).

[7]A. M. Baldin, Joint Institute for Nuclear Research Report JINR P1-11302, 1978.

[8]Y. D. Bayukov, V. I. Efremenko, S. Frankel, W. Frati, M. Gazzaly, G. A. Leksin, N. A. Nikiforov, C. F. Perdrisat, V. I. Tchistilin, and Y. M. Zaitsev, Phys. Rev. C **20**, 764 (1979).

[9]J. V. Geaga, S. A. Chessin, J. Y. Grossiord, J. W. Harris, D. L. Hendrie, L. S. Schroeder, R. N. Treuhaft, and K. Van Bibber, Phys. Rev. Lett. **45**, 1993 (1980).

[10]E. J. Moniz, I. Sick, R. R. Whitney, J. R. Ficenec, R. D. Kephart, and W. P. Trower, Phys. Rev. Lett. **26**, 445 (1971).

[11]S. Frankel, Phys. Rev. Lett. **38**, 1338 (1977).

[12]S. Gurvitz, Phys. Rev. Lett. **47**, 560 (1981).

[13]L. S. Schroeder, S. A. Chessin, J. V. Geaga, J. Y. Grossiord, J. W. Harris, D. L. Hendrie, R. Treuhaft, and K. Van Bibber, Phys. Rev. Lett. **43**, 1787 (1979).

[14]J. Cugnon, D. Kinet, and J. Vandermeulen, Nucl. Phys. **A379**, 553 (1982).

[15]C. L. Ruiz, R. W. Huggett, and P. N. Kirk, Nucl. Instrum. Methods **169**, 199 (1980).

[16]A. S. Goldhaber, Phys. Lett. **53B**, 306 (1974).

[17]C. Dols, Magnetic Measurements Group Report MT 21A, Lawrence Berkeley Laboratory, 1961.

[18]J. D. Dowell, W. F. Frisken, G. Martelli, B. Musgrave, H. B. Van De Ray, and R. Rubinstein, Nuovo Cimento **18**, 818 (1960).

[19]I. Tanihata (private communication).